

## Indication of Dynamic Peroxynitrite Fluctuations in the Rat Epilepsy Model with a Near-Infrared Two-Photon Fluorescent Probe

Xianzhu Luo, Ziyi Cheng, Rui Wang,\* and Fabiao Yu\*

Cite This: *Anal. Chem.* 2021, 93, 2490–2499

Read Online

ACCESS |



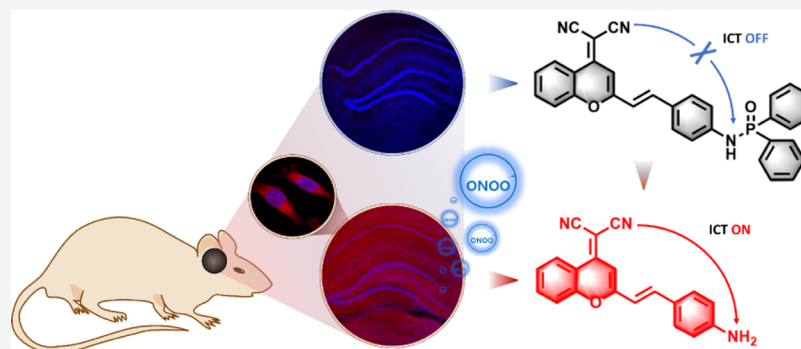
Metrics &amp; More



Article Recommendations



Supporting Information



**ABSTRACT:** Epilepsy is a chronic neurodegenerative disease that has seriously threatened human health. Accumulating evidence reveals that the pathological progression of epilepsy is closely related to peroxynitrite ( $\text{ONOO}^-$ ). Unfortunately, understanding the physiological roles of  $\text{ONOO}^-$  in epilepsy is still challenging due to the lack of powerful imaging probes for the determination of the level of fluctuations of  $\text{ONOO}^-$  in the epileptic brain. Herein, a near-infrared (NIR) two-photon (TP) fluorescent probe [dicyanomethylene-4*H*-pyran (DCM)- $\text{ONOO}^-$ ] is presented to trace  $\text{ONOO}^-$  in living cells and in kainate (KA)-induced rat epilepsy models with satisfactory sensitivity and selectivity. The probe is composed of a NIR TP DCM fluorophore and a recognition moiety diphenylphosphinamide. The phosphoramidate bond of the probe is interrupted after reacting with  $\text{ONOO}^-$  for 10 min, and then, the released amino groups emit strong fluorescence due to the restoration of the intramolecular charge transfer process. The probe can effectively detect the changes of endogenous  $\text{ONOO}^-$  with excellent temporal and spatial resolution in living cells and in rat epileptic brain. The imaging results demonstrate that the increasing level of  $\text{ONOO}^-$  is closely associated with epilepsy and severe neuronal damage in the brain under KA stimulation. In addition, the low-dose resveratrol can effectively inhibit  $\text{ONOO}^-$  overexpression and further relieve neuronal damage. With the assistance of TP fluorescence imaging in the epileptic brain tissue, we hypothesize that the abnormal levels of  $\text{ONOO}^-$  may serve as a potential indicator for the diagnosis of epilepsy. The TP fluorescence imaging based on DCM- $\text{ONOO}^-$  provides a great potential approach for understanding the epilepsy pathology and diagnosis.

## INTRODUCTION

Epilepsy is a chronic neurodegenerative disease that causes transient brain dysfunction.<sup>1</sup> About 50 million people in the world suffer from epilepsy, which is growing at a rate of 2–5 in 10,000 per year. More and more anti-epileptic drugs have recently been developed; these anti-epileptic drugs are only intended to prevent seizures, but cannot prevent the occurrence of epilepsy and electrogenesis after status epilepticus.<sup>2</sup> The increasing evidence indicates that epilepsy is closely associated with oxidative stress following high levels of reactive oxygen/nitrogen species (ROS/RNS).<sup>3</sup> Therefore, in order to comprehensively understand the epilepsy disease, it is necessary to investigate the role of oxidative stress in the epilepsy disease.

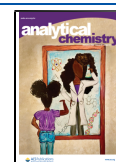
As a complex physiological process, epileptic seizure involves oxidative stress and mitochondrial dysfunction, which is

spontaneous, recurrent, and induces severe brain injury.<sup>4</sup> During the occurrence and development of epilepsy, the overexpressed ROS such as the superoxide anion ( $\text{O}_2^{\bullet-}$ ) are continuously generated and immediately react with nitric oxide (NO) to produce  $\text{ONOO}^-$ , which results in irreversible damage to a series of biological targets, such as DNA, lipids, and proteins and further causes neuronal cell death.<sup>5,6</sup> Thus, the overexpressed  $\text{ONOO}^-$  may be considered as an important indicator for the early diagnosis of epilepsy.<sup>7</sup> Unfortunately, the

Received: October 26, 2020

Accepted: January 4, 2021

Published: January 12, 2021



physiological roles of ONOO<sup>-</sup> are far from clearly understood yet. To investigate its crucial role in epilepsy, there is an urgent need to develop powerful imaging tools for detecting ONOO<sup>-</sup> in brain.

In recent years, fluorescent probes have become indispensable tools for studying biologically reactive molecules because of their advantages of high sensitivity, good selectivity, noninvasiveness, and excellent spatial and temporal resolution.<sup>8–12</sup> Several fluorescent probes for the detection of ONOO<sup>-</sup> in cells and *in vivo* have been reported;<sup>13–20</sup> however, the probes for specially monitoring ONOO<sup>-</sup> in epileptic brains are still challenging.<sup>21</sup> The emission of most reported fluorescent probes for ONOO<sup>-</sup> are located in the visible region, limiting the application for *in vivo* imaging. Therefore, near-infrared (NIR) fluorescent probes for monitoring ONOO<sup>-</sup> attracts more attention because of their unique advantages including deeper tissue penetration, less interference from background fluorescence, and less light damage.<sup>22–28</sup> Moreover, compared to the single-photon visible light region imaging, NIR two-photon (TP) microscopy can avoid autofluorescence and can reduce light damage.<sup>29–34</sup> However, most of the present TP probes suffer from an obstacle that these probes only can emit fluorescence with short wavelength (<550 nm), which may fail the bioimaging of brain tissues owing to light penetration depth and light scattering.<sup>35–37</sup> Therefore, there is a vital importance for a TP fluorescent probe with excitation/emission wavelength in the NIR region. With this aim in mind, we attempt to develop a TP fluorescence probe for the specific detection of ONOO<sup>-</sup> in living cells and *in vivo*, which could also track the fluctuations of ONOO<sup>-</sup> levels in epilepsy disease *in situ* and in real-time.

Herein, we presented a new NIR TP fluorescent probe DCM–ONOO for evaluating the critical physiological function and role of ONOO<sup>-</sup> in epilepsy. The probe comprised of the recognition moiety diphenylphosphinamide and NIR TP fluorophore dicyanomethylene-benzopyran (DCM). The probe exhibited specific response to ONOO<sup>-</sup> with a large Stokes shift, which satisfied sensitivity and selectivity, and released the NIR fluorescence signal at 685 nm depending on the mechanism of intramolecular charge transfer (ICT) process. DCM–ONOO could effectively track fluctuations of endogenous ONOO<sup>-</sup> levels in kainate (KA)-induced epileptic seizures. Furthermore, resveratrol could be employed as a potential anti-epilepsy agent to inhibit ONOO<sup>-</sup> overexpression and to relieve neuronal damage.

## EXPERIMENTAL SECTION

**Synthesis of Probe DCM–ONOO.** The synthesis and characterization of DCM–ONOO are displayed in [Supporting Information](#). Under argon (Ar) atmosphere, compound 5 (DCM–NH<sub>2</sub>, 0.31 g, 1 mmol), 0.1 mL of triethylamine, and 4-dimethylaminopyridine (0.12 g, 1 mmol) were added to a three-necked flask containing 20 mL of tetrahydrofuran at –10 °C. After stirring for 20 min, diphenylphosphinyl chloride (0.2 mL, 1 mmol) was added dropwise. The reaction continued for 2 h and then reacted at room temperature overnight. The solvent was removed under vacuum, and the crude product was obtained. It was then purified by silica gel chromatography (200–300 mesh) with the eluent CH<sub>2</sub>Cl<sub>2</sub>/ethyl acetate (10:1, v/v) to obtain the probe DCM–ONOO as a yellow solid (0.39 g, yield: 76%). The compound was accurately validated by nuclear magnetic resonance (<sup>1</sup>H NMR, <sup>13</sup>C NMR) and liquid chromatography high-resolution mass spectrometry (LC-

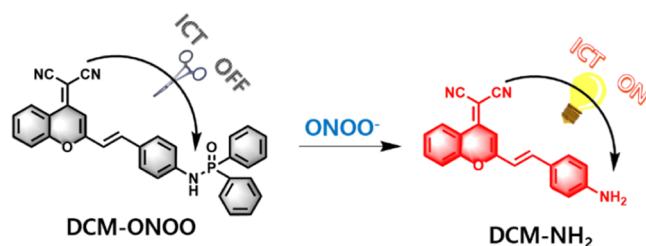
HRMS). <sup>1</sup>H NMR [400 MHz, dimethyl sulfoxide (DMSO)-*d*<sub>6</sub>]: δ (ppm) 10.14 (s, 1H), 8.75–8.73 (dd, 2H), 7.94–7.85 (m, 6H), 7.81–7.61 (m, 6H), 7.41–7.39 (dd, 1H), 7.29–7.25 (d, 2H), 7.07–6.96 (d, 2H), 6.87–6.85 (dd, 2H). <sup>13</sup>C NMR (100 MHz, DMSO-*d*<sub>6</sub>): δ (ppm) 167.4, 160.5, 159.4, 153.4, 152.5, 139.8, 135.8, 132.2, 132.0, 130.8, 130.5, 130.1, 129.1, 126.6, 125.1, 123.2, 119.5, 117.6, 116.5, 116.4, 106.2, 65.5. LC-HRMS (ESI, negative ion mode): *m/z* [C<sub>32</sub>H<sub>22</sub>N<sub>3</sub>O<sub>2</sub>P], calcd, 511.1450; found [M]: 511.1451 and [M – H]<sup>-</sup>: 510.1383.

**Establishment of Rat Epilepsy Model.** The SD rats were anesthetized by inhaling a certain amount of isoflurane, and the head was fixed on a brain stereotaxic instrument. After shaving the hair, iodine was used to partially disinfect. The scalp was cut along the midline of the rat's head, and then, the suprasquall key membrane and the cranial outer membrane were removed. The cornu ammonis 3 (CA3) area in the center of the right hippocampus was selected as the injection target (AP, –4.0 mm, ML, 4.40 mm, DV, 3.8 mm). After determining the location, a skull drill was used to drill through the skull to the dura, with caution so as not to damage the cortex. While drilling, the stereotaxic instrument was used to make the needle of the microsyringe penetrate 3.8 mm (subdural). 2.5 μL KA was slowly injected into the CA3 area of the hippocampus within 10 min, the needle was retained for 3 min, and the scalp was sutured after surgery. The severity of acute-stage seizures was graded according to grading standards. Rats with acute-stage seizures of grade IV and grade V were selected for the next pharmacological experiments. The specific classification of acute-stage seizures is described in [Supporting Information](#).

## RESULTS AND DISCUSSION

**Design and Synthesis of Probe DCM–ONOO.** The molecular structure of the probe and the proposed response mechanism of DCM–ONOO toward ONOO<sup>-</sup> are illustrated in [Scheme 1](#). To specially detect ONOO<sup>-</sup> fluctuations *in vivo*,

**Scheme 1.** Molecular Structure of DCM–ONOO and Its Proposed Response Mechanism toward ONOO<sup>-</sup>



the choice of a suitable fluorophore is of vital importance for the fluorescent probe that can be used in complex biological systems. DCM has been widely applied in the field of biological fluorescent imaging because of its unique advantages, including large Stokes shift, excellent light stability, NIR emission, and large TP absorption cross section.<sup>32,38</sup> Accordingly, a DCM derivative (DCM–NH<sub>2</sub>) is chosen to serve as the fluorescence signal transducer because of its stable spectroscopic properties in the range of biologically relevant pH. A fluorescent probe based on the nucleophilic cleavage of diphenyl phosphinate has been designed to detect ONOO<sup>-</sup>, providing a new strategy for detecting ONOO<sup>-</sup>.<sup>39,40</sup> It is hypothesized that phosphinamide-bond may be more stable than phosphinate, although it may not reduce the response rate

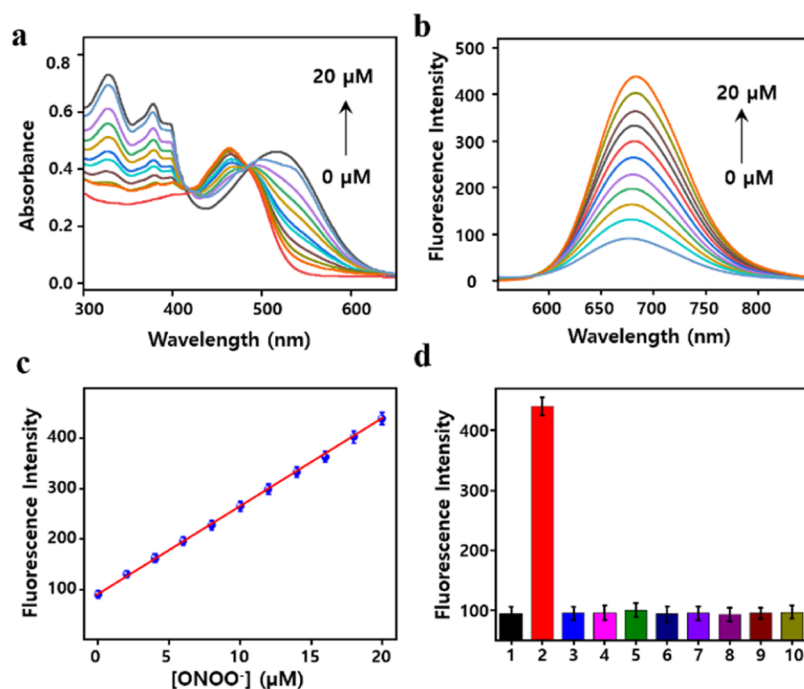


**Figure 1.** Spectral properties and selectivity of DCM-ONOO. (a) Dose-dependent UV-vis absorption spectrum with ONOO<sup>-</sup> (0–20 μM) for 10 min. (b) Fluorescence emission spectrum with ONOO<sup>-</sup> (0–20 μM), λ<sub>ex</sub> = 520 nm. (c) Linear relationship between the fluorescence intensity and different concentrations of ONOO<sup>-</sup>, λ<sub>ex</sub> = 520 nm, λ<sub>em</sub> = 685 nm. (d) fluorescent intensity response of DCM-ONOO to various reactive species at 10 min: 1, blank, 2, 20 μM ONOO<sup>-</sup>; 3, 100 μM NO<sub>2</sub><sup>-</sup>; 4, 100 μM NO; 5, 100 μM 100 μM NO<sub>3</sub><sup>-</sup>; 6, 100 μM OCl<sup>-</sup>; 7, 100 μM •OH; 8, 100 μM O<sub>2</sub><sup>•-</sup>; 9, 100 μM H<sub>2</sub>O<sub>2</sub>; 10, 100 μM <sup>t</sup>BuOO•. The experiments were repeated three times, and the data are shown as mean (±S.D.).

and selectivity. Inspired by this strategy, the diphenylphosphinamide as the response group was introduced to develop the NIR TP fluorescent probe to track the endogenous ONOO<sup>-</sup> fluctuations in the rat epilepsy model. As expected, the diphenylphosphinamide group exhibited high sensitivity, excellent selectivity, and rapid enough reaction dynamics toward ONOO<sup>-</sup>. Herein, a NIR TP fluorescence probe triggered by ONOO<sup>-</sup> is synthesized *via* combining DCM-NH<sub>2</sub> with diphenylphosphinyl chloride (Scheme S1). The integration of the response group prevents the ICT process of the fluorophore. The reaction of ONOO<sup>-</sup> can cleave the phosphoramidate bond and release the free amino-fluorophore, which induces the recovery of the ICT process, thereby providing a characteristic fluorescence emission peak centered at 685 nm in the NIR region.

**Spectroscopic Properties.** The spectral properties of DCM-ONOO were evaluated in phosphate-buffered saline (PBS) buffer (10 mM, pH = 7.4, 30% DMSO). As depicted in Figure 1a, the probe provided a strong absorption centered at 460 nm. With the treatment of ONOO<sup>-</sup> (0–20 μM), there was a large 52 nm redshift to 512 nm, because the phosphoramidate bond was interrupted and the fluorophore DCM-NH<sub>2</sub> was released (Figure 1a). Simultaneously, the fluorescence response of DCM-ONOO (10 μM) to different concentrations of ONOO<sup>-</sup> was examined. The probe DCM-ONOO was accompanied by a large Stokes shift of 165 nm, and its fluorescence intensity of probe DCM-ONOO centered at 685 nm gradually increased, which should be due to the cleaved phosphoramidate bond by ONOO<sup>-</sup> (Figure 1b). In order to verify this conjecture, the high-performance liquid chromatography (HPLC) experiment was performed. As shown in Figure S1, the peaks of DCM-ONOO and DCM-NH<sub>2</sub> are located at 4.46 min and 6.87 min, respectively. With

the addition of ONOO<sup>-</sup>, a new peak appeared in the probe solution, which happened to coincide with the retention time of DCM-NH<sub>2</sub>. These results indicated that ONOO<sup>-</sup> could smartly break the phosphoramidate bond of the probe and could switch a significant fluorescent signal on. Furthermore, a satisfactory linear relationship between the fluorescence intensities and ONOO<sup>-</sup> concentrations from 0–20 μM was obtained (Figure 1c). The regression equation was  $F_{520\text{nm}} = 17.1270 \times [\text{ONOO}^-] \mu\text{M} + 93.4746$  with a linear fitting constant  $r = 0.9993$ . Based on the standard method of  $3\sigma/k$ , the limit of detection was calculated to be 96 nM. Besides, the experimental detection limit was estimated to be 151 nM. These results indicated that the probe could potentially serve as a powerful detection tool to quantitatively and qualitatively identify trace ONOO<sup>-</sup> *in vitro*.

**Selectivity and Response Time.** The desirable fluorescent probes generally possess high stability and excellent selectivity in the physiological pH range. Because of the instability of ONOO<sup>-</sup> in biological systems, the reaction dynamics of DCM-ONOO on ONOO<sup>-</sup> was investigated. Compared with the absence of ONOO<sup>-</sup>, the fluorescence signal reached its maximum value in about 10 min, which suggested that the probe was able to quickly respond to ONOO<sup>-</sup> and the possibility of further applying to the real-time imaging of ONOO<sup>-</sup> in living cells (Figure S2). High selectivity is crucial to evaluate the probe's usability in the complexity of the biological environment. The response of DCM-ONOO was investigated toward various biological interferents, including ROS/RNS: NO<sub>2</sub><sup>-</sup>; NO; HNO; OCl<sup>-</sup>; •OH; O<sub>2</sub><sup>•-</sup>; H<sub>2</sub>O<sub>2</sub>; <sup>t</sup>BuOO•, ions and anions: Na<sup>+</sup>; K<sup>+</sup>; Ca<sup>2+</sup>; H<sub>2</sub>PO<sub>4</sub><sup>-</sup>; SO<sub>3</sub><sup>2-</sup>; HCO<sub>3</sub><sup>-</sup>; HS<sup>-</sup>, and biothiols: glutathione (GSH); cysteine; homocysteine. It was delightful that only ONOO<sup>-</sup> induced significant fluorescence enhancement because it could

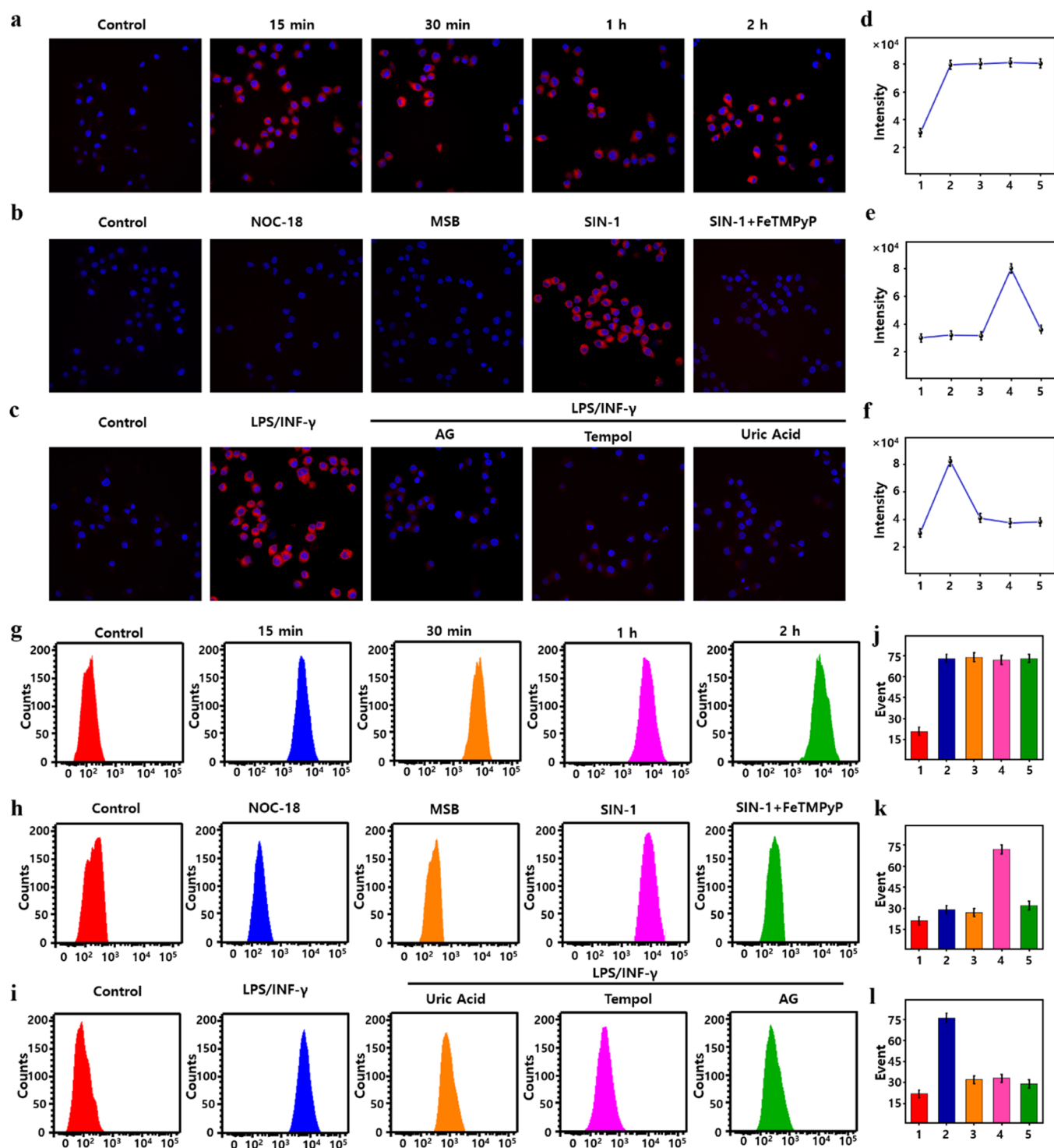


**Figure 2.** Imaging of endogenous and exogenous  $\text{ONOO}^-$  in RAW 264.7 cells. (a) Fluorescent imaging of  $\text{ONOO}^-$  generation in RAW 264.7 cells at time points: 0, 15, 30 min, and 1 and 2 h. (b) Fluorescent imaging of exogenous  $\text{ONOO}^-$  in RAW 264.7 cells. (c) Fluorescent imaging of endogenous  $\text{ONOO}^-$  in RAW 264.7 cells. (d–f) Mean fluorescence intensities of images in (a–c). (g–i) Flow cytometry analysis for (a–c). (j–l) Mean values of (g–i). Confocal microscopy images ( $\lambda_{\text{ex}} = 820 \text{ nm}$ ,  $\lambda_{\text{em}} = 650\text{--}730 \text{ nm}$ ) and flow cytometry assays ( $\lambda_{\text{ex}} = 514 \text{ nm}$ ,  $\lambda_{\text{em}} = 650\text{--}730 \text{ nm}$ ) for the detection of  $\text{ONOO}^-$  in RAW 264.7 cells. The experiments were repeated three times, and the data are shown as mean ( $\pm$ S.D.).

efficiently trigger the probe to release the free  $\text{DCM-NH}_2$  fluorophore, further verifying that  $\text{DCM-ONOO}$  exhibited excellent selectivity to  $\text{ONOO}^-$  (Figures 1d and S3). Moreover, we also assessed the fluorescence intensity changes of some interferers ( $\text{O}_2^{\bullet-}$ ,  $-\text{OH}$ , and  $\text{NO}$ ) in 0 – 60 min (Figure S4), which caused negligible fluorescence signal changes. To estimate the effect of pH on  $\text{DCM-ONOO}$  in

the absence and presence of  $\text{ONOO}^-$ , their fluorescence intensity was analyzed at  $\lambda_{\text{em}} = 685 \text{ nm}$  ranging from pH 3.0 – 10.0. As shown in Figure S5, there was negligible fluorescence change at the maximum emission (685 nm) for  $\text{DCM-ONOO}$  with an excitation at 520 nm, indicating the high stability of the probe. Upon the addition of  $\text{ONOO}^-$ , a significant increase of fluorescence intensity at 685 nm was

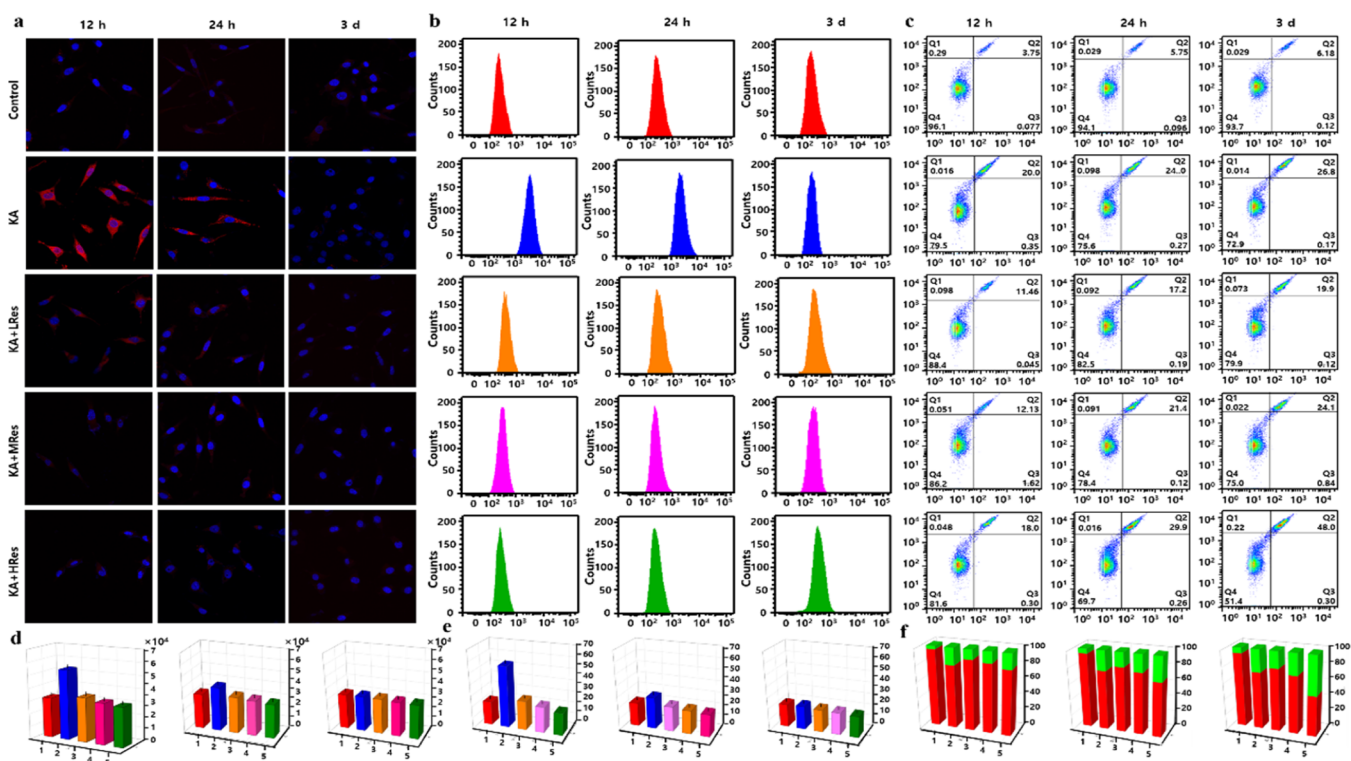


**Figure 3.** Detection of  $\text{ONOO}^-$  fluctuation in living HT22 cells with DCM-ONOO by confocal microscopic imaging and flow cytometry analysis. Confocal microscopy images ( $\lambda_{\text{ex}} = 820 \text{ nm}$ ,  $\lambda_{\text{em}} = 650\text{--}730 \text{ nm}$ ) and flow cytometry assays ( $\lambda_{\text{ex}} = 514 \text{ nm}$ ,  $\lambda_{\text{em}} = 650\text{--}730 \text{ nm}$ ) for the detection of  $\text{ONOO}^-$  in HT22 cells. The HT22 cells were treated with KA ( $50 \mu\text{M}$ , 12, 24 h, and 3 d), KA + LRes ( $20 \mu\text{M}$ , 12, 24 h, and 3 d), KA + MRes ( $50 \mu\text{M}$ , 12, 24 h, and 3 d), and KA + HRes ( $100 \mu\text{M}$ , 12, 24 h, and 3 d), respectively. Consequently, DCM-ONOO ( $10 \mu\text{M}$ ) incubated for 15 min at  $37^\circ\text{C}$  before confocal imaging and flow cytometry analyses. (a) Fluorescent imaging of  $\text{ONOO}^-$  in different HT22 model cells. (b) Flow cytometry analysis for a. (c) Apoptosis detection by flow cytometry analysis. Q1: necrosis cells, Q2: late apoptotic cells, Q3: early apoptotic cells, Q4: survival cells. (d) Mean fluorescence intensities of the images in (a). (e) Mean values of (b). (f) Apoptosis rate. The data are shown as mean ( $\pm\text{S.D.}$ ).

observed in the pH from 4.8 to 7.0 and then reached a plateau, demonstrating that DCM-ONOO could be utilized to monitor  $\text{ONOO}^-$  under the physiological pH range. The maximal TP absorption cross section of DCM-ONOO was measured as 48 GM with excitation wavelength at 820 nm *via* reported methods, which suggested that the TP microscope could be employed to track  $\text{ONOO}^-$  in living cells.<sup>34</sup>

**Imaging of  $\text{ONOO}^-$  in Living Cells.** Encouraged by the prominent chemical performance of DCM-ONOO, we further assessed the potential application of this probe to detect  $\text{ONOO}^-$  in living cells. To verify the biocompatibility of this probe, the cytotoxicity of DCM-ONOO was evaluated by Cell Counting Kit-8 (CCK-8) assay against mouse mononuclear macrophage cell line (RAW 264.7 cells) and mouse hippocampal (HIP) neuron cell line (HT22 cells). As illustrated in Figure S6, the probe exhibited low cytotoxicity and high biocompatibility.

Because the probe possessed the features of low cytotoxicity, high sensitivity, as well as high specificity, we hypothesized that DCM-ONOO could be suitable for the detection of  $\text{ONOO}^-$  in living cells. Afterward, the RAW 264.7 cell line was selected as the testing cell model. First, the optimal incubation time was examined after adding the probe DCM-ONOO ( $10 \mu\text{M}$ ) to RAW 264.7 cells. The RAW 264.7 cells were incubated for 1 h in the absence or presence of  $100 \mu\text{M}$  3-morpholino-sydnonimine (SIN-1, an  $\text{ONOO}^-$  donor) and then treated with DCM-ONOO ( $10 \mu\text{M}$ ) before imaging. As illustrated in Figure 2a, a weak fluorescence signal was obtained in RAW

264.7 cells without pretreatment with SIN-1. In contrast, after the cells were incubated with SIN-1 for 15 min, a significant fluorescence was observed and attained saturation; thus the best incubation time was set to be 15 min. Furthermore, the probe could maintain fluorescence in the cells for 2 h. Subsequently, flow cytometry assays were employed to further verify these data. As shown in Figure 2g,j, the results were in well accordance with the imaging output (Figure 2a,d). Subsequently, in order to prove that the probe could respond specifically to  $\text{ONOO}^-$  in living cells, NOC-18 (a NO donor,  $500 \mu\text{M}$ ) and MSB (a  $\text{O}_2^{\bullet-}$  donor,  $100 \mu\text{M}$ ) were employed for real-time generation of  $\text{ONOO}^-$ .<sup>41</sup> As expected, no evident intracellular fluorescence signals were observed. Moreover, a dramatic fluorescence signal was obtained by the treatment with SIN-1, but the treatment with FeTMPyP (a  $\text{ONOO}^-$  decomposition catalyst,  $50 \mu\text{M}$ ) could effectively suppress the generation of fluorescence (Figure 2b).<sup>42</sup> These results suggested that only  $\text{ONOO}^-$  could trigger the fluorescence turn-on response rather than other substances, which further indicated the specific imaging of  $\text{ONOO}^-$  with DCM-ONOO in living cells. These observations were confirmed by flow cytometry analyses. As shown in Figure 2h,k, the obtained results were basically consistent with the above imaging outcome. The potential of DCM-ONOO for imaging endogenous  $\text{ONOO}^-$  was investigated in living cells. The assays were performed in RAW 264.7 cells because the cells expressed high levels of inducible nitric oxide synthase (NOS) after being stimulated by lipopolysaccharide (LPS,  $1 \mu\text{g}/\text{mL}$ )/

interferon- $\gamma$  (INF- $\gamma$ , 100 ng/mL).<sup>43</sup> A significant fluorescence enhancement in RAW 264.7 cells was found by the treatment with LPS/INF- $\gamma$ , which demonstrated that the intracellular ONOO<sup>-</sup> level increased under the stimulation of external oxidative stress.

However, the living cells were stimulated with LPS/INF- $\gamma$  and pretreated with a NOS inhibitor aminoguanidine (0.5 mM), a superoxide scavenger 2,2,6,6-tetramethylpiperidine-*N*-oxyl (Tempol, 0.5 mM), or a ONOO<sup>-</sup> scavenger (uric acid, 100  $\mu$ M) and then treated with DCM-ONOO, because of which the intracellular fluorescence signals were greatly inhibited, suggesting that the levels of intracellular ONOO<sup>-</sup> were decreased.<sup>14</sup> Meanwhile, it also indicated that the detected intracellular fluorescence signals were indeed caused by the endogenous ONOO<sup>-</sup> rather than other ROS (Figure 2c). The obtained data were further verified by flow cytometry analysis. As shown in Figure 2i,j, the observed results were well consistent with fluorescence images (Figure 2c,f). All the above results indicated that the probe DCM-ONOO could be suitable for monitoring of endogenous and exogenous ONOO<sup>-</sup> in living cells.

**Visualizing of ONOO<sup>-</sup> Levels in HT22 Cells under KA Stimulation.** Because the probe had been successfully employed to detect ONOO<sup>-</sup> in living cells, we tried to further investigate the fluctuations of ONOO<sup>-</sup> concentrations in cells under KA stimulation. Resveratrol (Res), a small molecule of polyphenols, possesses a strong antioxidant effect, which can play biological roles by activating histone deacetylase. Furthermore, recent studies reported that Res is able to effectively reduce nerve damage.<sup>44</sup> Therefore, we attempted to explore the effect of Res on the expression of ONOO<sup>-</sup> under KA stimulation. Herein, a nerve cell line HT22 cell line was selected as the test cell model. In this assay, the cells were divided into five groups, and each group was imaged after the cells were incubated for 12, 24, and 72 h, respectively. Control group: HT22 cells. KA group: HT22 cells were incubated with KA (50  $\mu$ M). HT22 cells were treated with KA (50  $\mu$ M) and Res (low-dose, LRes, 20  $\mu$ M), Res (medium-dose, MRes, 50  $\mu$ M), and Res (high-dose, HRes, 100  $\mu$ M) as KA + LRes, KA + MRes and KA + HRes, respectively. As illustrated in Figure 3a, the control group provided weak fluorescent signals, revealing low levels of ONOO<sup>-</sup> in HT22 cells. However, the KA group displayed relatively powerful fluorescent signals, further indicating the increased ONOO<sup>-</sup> content under KA stimulation. Compared with the KA group, the treatment with different concentrations of Res resulted in nearly invisible fluorescence, indicating that the concentration of ONOO<sup>-</sup> was low, which should be the result of certain antioxidant effects of Res. Evidently, the fluorescence intensity of the KA + HRes group was lower, revealing that the inhibitory effect of high-dose Res was better than that of low-dose Res. Along with the extent time to 24 h, only the KA group still possessed stronger fluorescence. Nevertheless, the other groups displayed lower fluorescence, which demonstrated that Res could inhibit the overexpression of ONOO<sup>-</sup>. However, with an extended time period of 3 days, cells in all the groups exhibited negative fluorescence intensity. These above results demonstrated that Res might be applied to relieve the oxidative stress caused by KA. Subsequently, flow cytometry analysis was also performed (Figure 3b,e) that showed excellent consistency with the outcomes of bioimaging (Figure 3a,d). In addition, compared to the control group, the cells in other groups were clearly round and in a semi-adherent state, especially the KA group

and the KA + HRes in 3 days (Figure 3a). The result suggested that the addition of KA and high-dose of Res might induce apoptosis. Thus, the disturbance of redox homeostasis inevitably led to cell apoptosis. On the basis of these phenomena, the apoptosis experiment was carried out *via* a flow cytometry approach. As illustrated in Figure 3c,f, the apoptosis rates of the KA groups increased compared with that of the control groups. The ratio of apoptotic cells in the KA + LRes and KA + MRes groups were lower than that of the KA group. However, KA + HRes groups displayed the opposite trend, which exactly coincided with the poor state of the cells that we observed in this group. These results indicated that high-dose Res could not improve the disorder of intracellular redox homeostasis caused by KA, which further aggravated apoptosis; in contrast, low-dose Res could scavenge RNS with less damage to cells. Taken together, the developed fluorescent probe DCM-ONOO would effectively investigate the fluctuation of intracellular ONOO<sup>-</sup> in living cells and evaluate the role of Res inhibiting the overproduction of endogenous ONOO<sup>-</sup> under KA stimulation. The probe could be used for simple screening of inducers and inhibitors against the formation of ONOO<sup>-</sup> according to the changes in its fluorescence signal.

**Visualizing Real-Time Imaging of Endogenous ONOO<sup>-</sup> in Rats.** With the promising living cell imaging data in hand, we next assessed the suitability of DCM-ONOO for the detection of ONOO<sup>-</sup> *in vivo*. Generally, rats were divided into four groups. For the control group, the rats were processed with an intraperitoneal (i.p.) injection of PBS buffer before intravenous (i.v.) injection of probe DCM-ONOO. The other groups were pretreated with SIN-1, SIN-1 + Res, and SIN-1 + uric acid by i.p. injection, respectively. Subsequently, the images were captured at different time points (5, 15, 30, 45, and 60 min) after i.v. injection of probe DCM-ONOO. As shown in Figure S7, weak fluorescence intensity was obtained in the control group, implying that the ONOO<sup>-</sup> content was low under normal circumstances. In contrast, SIN-1 groups displayed powerful NIR fluorescence signals, which were gradually increasing within 30 min and then remained at the maximum intensity for a period of time. The results indicated that the probe could be applied for real-time imaging of ONOO<sup>-</sup> *in vivo*. Thereafter, an ONOO<sup>-</sup> scavenger (uric acid) was employed to verify whether fluorescence was induced by an increase in the amount of ONOO<sup>-</sup> *in vivo*. Negligible fluorescence signals were observed as compared with SIN-1 groups, further revealing that the probe DCM-ONOO could be utilized to image and monitor the fluctuations of ONOO<sup>-</sup> *in vivo*. Meanwhile, weak fluorescence signals were also obtained for the rats pretreated with Res before SIN-1 administration, confirming that Res could effectively inhibit the excessive increase of ONOO<sup>-</sup>, which should be because of the antioxidant effect of Res. The above results demonstrated DCM-ONOO offered great potential to serve as a chemical tool for tracing ONOO<sup>-</sup> *in vivo* and Res might be used as an antioxidant drug.

**Imaging of ONOO<sup>-</sup> in Rat Epilepsy Models.** Encouraged by the above results, we further explored whether DCM-ONOO could be applied to the fluctuation of endogenous ONOO<sup>-</sup> levels in the epileptic brain. The concentration of ONOO<sup>-</sup> in healthy brains is about 300 nM, and its concentration would obviously increase in epilepsy disease.<sup>21</sup> The proposed probe was sensitive enough to detect the ONOO<sup>-</sup> levels in epilepsy. Herein, the KA-induced method, a

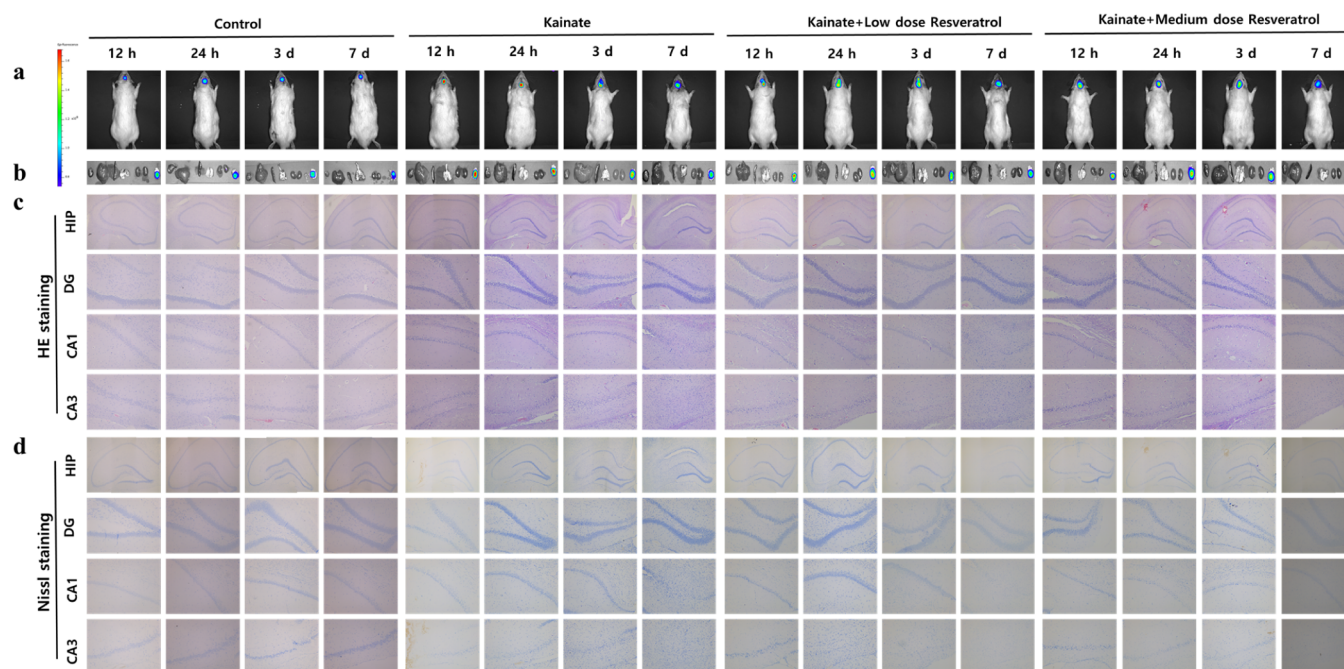


**Figure 4.** Time-dependent fluorescence images of rat epilepsy models ( $\lambda_{\text{ex}} = 514 \text{ nm}$ ,  $\lambda_{\text{em}} = 650\text{--}730 \text{ nm}$ ). (a) Fluorescence images of  $\text{ONOO}^-$  with DCM-ONOO in the hippocampus of normal, epilepsy, and treatment rats. (b) Fluorescence detection of vitro vital organs (heart, liver, spleen, lung, kidney, and brain) from the rats in (a). (c) HE and (d) Nissl staining for evaluating neuronal damage in the HIP region.

classic model of induced epilepsy in rat, was employed. Rats were divided into five groups: Control group: normal rats; KA group: rat epileptic model; KA + LRes group, KA + MRes group, and KA + HRes group. The rats were pretreated with different doses of Res (15, 30, and 60 mg/kg/d) after the same procedure as that of the KA group, respectively. Unfortunately, almost all the rats in the KA + HRes group died, which might be due to the high concentration of Res causing certain toxic and side effects.

Herein, rats with grade IV and grade V acute attacks were selected for the following experiments. All the rats were treated with intracranial injection of DCM-ONOO ( $50 \mu\text{M}$ ,  $50 \mu\text{L}$  in DMSO/saline = 1:99, v/v) for 30 min before *in vivo* fluorescence imaging. As illustrated in Figure 4a, all control groups exhibited weak fluorescence signal, implying that the content of  $\text{ONOO}^-$  in normal rats was quite low. However, compared with other groups, the fluorescence intensity of the KA group was significantly stronger in 12 h, indicating a higher  $\text{ONOO}^-$  content, which further verified that epilepsy would cause abnormal elevation of  $\text{ONOO}^-$  levels. The fluorescence intensity of the KA + LRes group and the KA + MRes group were relatively weaker than that of the KA group, revealing that the  $\text{ONOO}^-$  content reduced after Res treatment, which should be attributed to the antioxidant effect of Res. Subsequently, the fluctuations of  $\text{ONOO}^-$  content within a week (quiescent period) were assessed. The fluorescence intensity of each group decreased and tended to stabilize with the extension of time, indicating that the content of  $\text{ONOO}^-$  increased during the seizure of rats, but it could gradually decrease or even return to the original state during the stable period, such as 3 days and 7 days. In addition, different organs were collected and then subjected to fluorescence imaging analysis (Figure 4b). Except for the brain, no obvious fluorescence intensity was found in the lung, heart, spleen, liver, and kidney. The phenomenon of *in vitro* and *in vivo* experiments was almost identical. These results implied that

the occurrence of epilepsy disease might be inseparable from  $\text{ONOO}^-$ . Meanwhile, it also confirmed that Res was effective for the treatment of epilepsy. Thus,  $\text{ONOO}^-$  might be used as an indicator of epilepsy disease and a potential chemical and biological imaging tool for diagnosis of epilepsy disease. The probe can be utilized as a screening agent for antioxidant drugs. Excessive  $\text{ONOO}^-$  produced by stimulating stress may further lead to severe neuronal death, which is also closely related to the decrease of GSH peroxidase and protective superoxide dismutase 2 in epilepsy diseases.<sup>3</sup> Consequently, epilepsy is often accompanied by damage to HIP neurons. The hematoxylineosin and Nissl staining were employed to illustrate the pathological morphology of the epilepsy and to verify whether the rat epilepsy model was successfully established or not (Figure 4c,d). The neurons in the cornu ammonis 1 (CA1), CA3, and dentate gyrus (DG) regions of the hippocampus of the control group were polygonal, the nuclei were lightly stained and vacuolated, with clear nucleoli, basophilic cytoplasm, and no abnormalities in the neural network. Interestingly, no significant neuron loss was observed in the DG region of all groups. However, in the KA group, a large number of neurons were lost and fewer residual neurons, followed by the KA + MRes group, and a small number of neurons were lost and more residual neurons in the KA + LRes group. The neuron layer in the HIP CA3 area further thinned and neurons were again lost in 24 h. Subsequently, we observed that about 3 d after the injection of KA, a large number of CA3 neuronal cells degenerated and died in the rats. The loss of neurons in the CA1 and CA3 regions of the hippocampus in the KA group and the KA + MRes group was severe, and almost no neurons remained, but there was neuron loss in HIP CA3 but no obvious abnormalities in CA1 area in the KA + LRes group at 7 days. The above results suggested that the KA + LRes group possessed a better protective effect on neurons in the HIP CA1 area than the CA3 area. Compared with the KA + LRes group, the KA + MRes group exhibited a

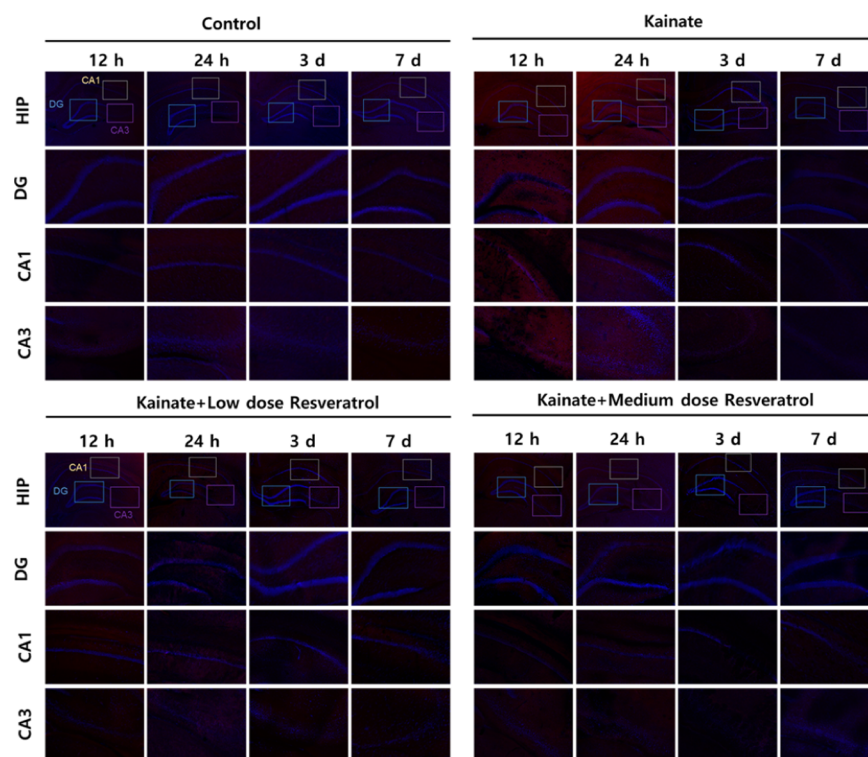


**Figure 5.** Fluorescent brain tissue imaging was performed to assess the levels of  $\text{ONOO}^-$  dynamic changes and neuronal damage for whole HIP region, CA1, CA3, and DG subregions at different times in various rat models after KA administration. Red channel: DCM-ONOO with collection window from 650 nm to 730 nm ( $\lambda_{\text{ex}} = 820 \text{ nm}$ ); Blue channel: 4',6-diamidino-2-phenylindole.

poor protective effect on neurons, which further suggested that the low concentration of Res had a certain protective effect on neurons. Overall, after the application of Res drugs, the early and mid-term (12, 24 h, and 3 d) had a trend of delaying neuronal degeneration or protecting neurons, and the low-dose had a more obvious effect than the high dose.

To further discuss the level changes of  $\text{ONOO}^-$ , fluorescence imaging of the fresh rat brain slices was carried out (Figure 5). The brain tissue slices were incubated with DCM-ONOO ( $10 \mu\text{M}$ ) for 20 min and then washed with PBS three times before TP confocal fluorescence imaging (Figure 5). In the control group, the fluorescence signal in each area of the hippocampus exhibited weak fluorescence signals, clear hierarchical structure, neatly arranged nerve cells, and uniform cytoplasmic staining. However, KA group's tissues exhibited strong fluorescence, especially in CA1 and CA3 regions. In addition, a large number of neuron loss and disorder were observed, which should be attributed to the overdose of  $\text{ONOO}^-$ . The fluorescence intensity of the KA + LRes group and KA + MRes group were significantly weaker than the KA group. As shown in Figure 5, the fluctuations of fluorescence signals were consistent with the results in Figure 4a. The above assays displayed that the probe possessed favorable penetration ability and could be utilized for  $\text{ONOO}^-$  detecting and imaging in tissue and *in vivo*. All of these observations demonstrated that overexpressed  $\text{ONOO}^-$  might induce severe neuronal damage and even death, while effective inhibition of  $\text{ONOO}^-$  in the brain might have the potential to be a useful strategy for relieving epilepsy.

## CONCLUSIONS

In summary, we developed a new NIR TP fluorescent probe DCM-ONOO to track the dynamic changes of  $\text{ONOO}^-$  in live cells and *in vivo*. The probe features high sensitivity and specificity as well as rapid detection toward  $\text{ONOO}^-$  in virtue of the supervision of the ICT mechanism. Combining with TP fluorescence imaging, DCM-ONOO can effectively visualize the endogenous  $\text{ONOO}^-$  in the hippocampus region of KA-induced epileptic rat model, demonstrating the positive correlation between abnormal overexpressed  $\text{ONOO}^-$  and epilepsy seizures as well as the neuronal damage. Furthermore, resveratrol can effectively inhibit the overexpression of  $\text{ONOO}^-$  and the damage of neurons, which has the potential use for the remission of epilepsy. The probe DCM-ONOO may provide great potential to serve as a powerful chemical tool for real-time tracking of  $\text{ONOO}^-$  fluctuations and further assist diagnosis of epilepsy diseases.

## ASSOCIATED CONTENT

### Supporting Information

The Supporting Information is available free of charge at <https://pubs.acs.org/doi/10.1021/acs.analchem.0c04529>.

More experimental materials, general methods, additional figures, synthesis steps, and compound characterization, procedure for the synthesis of the probe, spectrum for structure characterizations, HPLC experiments, and additional fluorescence spectra and images (PDF)

## AUTHOR INFORMATION

## Corresponding Authors

**Rui Wang** – Key Laboratory of Emergency and Trauma, Ministry of Education, Key Laboratory of Hainan Trauma and Disaster Rescue, The First Affiliated Hospital of Hainan Medical University, Institute of Functional Materials and Molecular Imaging, College of Emergency and Trauma, Hainan Medical University, Haikou 571199, China; Email: wangrui@hainmc.edu.cn

**Fabiao Yu** – Key Laboratory of Emergency and Trauma, Ministry of Education, Key Laboratory of Hainan Trauma and Disaster Rescue, The First Affiliated Hospital of Hainan Medical University, Institute of Functional Materials and Molecular Imaging, College of Emergency and Trauma, Hainan Medical University, Haikou 571199, China; [orcid.org/0000-0003-0073-6299](https://orcid.org/0000-0003-0073-6299); Email: yufabiao@hainmc.edu.cn

## Authors

**Xianzhu Luo** – Key Laboratory of Emergency and Trauma, Ministry of Education, Key Laboratory of Hainan Trauma and Disaster Rescue, The First Affiliated Hospital of Hainan Medical University, Institute of Functional Materials and Molecular Imaging, College of Emergency and Trauma, Hainan Medical University, Haikou 571199, China

**Ziyi Cheng** – Key Laboratory of Emergency and Trauma, Ministry of Education, Key Laboratory of Hainan Trauma and Disaster Rescue, The First Affiliated Hospital of Hainan Medical University, Institute of Functional Materials and Molecular Imaging, College of Emergency and Trauma, Hainan Medical University, Haikou 571199, China

Complete contact information is available at:

<https://pubs.acs.org/10.1021/acs.analchem.0c04529>

## Notes

The authors declare no competing financial interest.

## ACKNOWLEDGMENTS

This work was supported by the Hainan Provincial High-level Talent Project (Nos. 2019RC210 and 2019RC220), National Natural Science Foundation of China (Nos. 21775162, 21864011, and 22064009), Hainan Key Research and Development Project (Grant ZDYF2020133), CAMS Innovation Fund for Medical Sciences (2019-I2M-5-023), Nanhai Young-Talent Program of Hainan (Grant. 20202007), and Hundred Talent Program of Hainan (2018).

## REFERENCES

- (1) Moshé, S. L.; Perucca, E.; Rylvlin, P.; Tomson, T. *Lancet* **2015**, *385*, 884–898.
- (2) Löscher, W.; Klitgaard, H.; Twyman, R. E.; Schmidt, D. *Nat. Rev. Drug Discovery* **2013**, *12*, 757–776.
- (3) Chuang, Y.-C.; Chen, S.-D.; Liou, C.-W.; Lin, T.-K.; Chang, W.-N.; Chan, S. H. H.; Chang, A. Y. W. *Epilepsia* **2009**, *50*, 731–746.
- (4) Kwan, P.; Brodie, M. J. *N. Engl. J. Med.* **2000**, *342*, 314–319.
- (5) Sedgwick, A. C.; Han, H.-H.; Gardiner, J. E.; Bull, S. D.; He, X.-P.; James, T. D. *Chem. Sci.* **2018**, *9*, 3672–3676.
- (6) Reverte, M.; Vaissiere, A.; Boisguerin, P.; Vasseur, J.-J.; Smietana, M. *ACS Sens.* **2016**, *1*, 970–974.
- (7) Bezner, B. J.; Ryan, L. S.; Lippert, A. R. *Anal. Chem.* **2020**, *92*, 309–326.
- (8) Sun, W.; Guo, S.; Hu, C.; Fan, J.; Peng, X. *Chem. Rev.* **2016**, *116*, 7768–7817.

- (9) Cheng, D.; Peng, J.; Lv, Y.; Su, D.; Liu, D.; Chen, M.; Yuan, L.; Zhang, X. *J. Am. Chem. Soc.* **2019**, *141*, 6352–6361.
- (10) Zhang, J.; Chai, X.; He, X.-P.; Kim, H.-J.; Yoon, J.; Tian, H. *Chem. Soc. Rev.* **2019**, *48*, 683–722.
- (11) Li, X.; Gao, X.; Shi, W.; Ma, H. *Chem. Rev.* **2014**, *114*, 590–659.
- (12) Cao, D.; Liu, Z.; Verwilt, P.; Koo, S.; Jangjili, P.; Kim, J. S.; Lin, W. *Chem. Rev.* **2019**, *119*, 10403–10519.
- (13) Sun, X.; Xu, Q.; Kim, G.; Flower, S. E.; Lowe, J. P.; Yoon, J.; Fossey, J. S.; Qian, X.; Bull, S. D.; James, T. D. *Chem. Sci.* **2014**, *5*, 3368–3373.
- (14) Peng, T.; Wong, N.-K.; Chen, X.; Chan, Y.-K.; Ho, D. H.-H.; Sun, Z.; Hu, J. J.; Shen, J.; El-Nezami, H.; Yang, D. *J. Am. Chem. Soc.* **2014**, *136*, 11728–11734.
- (15) Kim, J.; Park, J.; Lee, H.; Choi, Y.; Kim, Y. *Chem. Commun.* **2014**, *50*, 9353–9356.
- (16) Cheng, D.; Xu, W.; Yuan, L.; Zhang, X. *Anal. Chem.* **2017**, *89*, 7693–7700.
- (17) Li, H.; Li, X.; Wu, X.; Shi, W.; Ma, H. *Anal. Chem.* **2017**, *89*, 5519–5525.
- (18) Zhou, X.; Kwon, Y.; Kim, G.; Ryu, J.-H.; Yoon, J. *Biosens. Bioelectron.* **2015**, *64*, 285–291.
- (19) Liu, C.; Zhang, X.; Li, Z.; Chen, Y.; Zhuang, Z.; Jia, P.; Zhu, H.; Yu, Y.; Zhu, B.; Sheng, W. *J. Agric. Food Chem.* **2019**, *67*, 6407–6413.
- (20) Liu, C.; Duan, Q.; Zhang, X.; Li, Z.; Jia, P.; Zhu, H.; Yu, Y.; Wang, Z.; Zhu, B.; Sheng, W. *Sens. Actuators, B* **2019**, *289*, 124–130.
- (21) Hu, J. S.; Shao, C.; Wang, X.; Di, X.; Xue, X.; Su, Z.; Zhao, J.; Zhu, H. L.; Liu, H. K.; Qian, Y. *Adv. Sci.* **2019**, *6*, 1900341.
- (22) Zhu, B.; Zhang, M.; Wu, L.; Zhao, Z.; Liu, C.; Wang, Z.; Duan, Q.; Wang, Y.; Jia, P. *Sens. Actuators, B* **2018**, *257*, 436–441.
- (23) Yu, F.; Li, P.; Wang, B.; Han, K. *J. Am. Chem. Soc.* **2013**, *135*, 7674–7680.
- (24) Li, J.; Lim, C. S.; Kim, G.; Kim, H. M.; Yoon, J. *Anal. Chem.* **2017**, *89*, 8496–8500.
- (25) Jiang, W.-L.; Li, Y.; Wang, W.-X.; Zhao, Y.-T.; Fei, J.; Li, C.-Y. *Chem. Commun.* **2019**, *55*, 14307–14310.
- (26) Li, D.; Wang, S.; Lei, Z.; Sun, C.; El-Toni, A. M.; Alhoshan, M. S.; Fan, Y.; Zhang, F. *Anal. Chem.* **2019**, *91*, 4771–4779.
- (27) Liu, D.; Feng, S.; Feng, G. *Sens. Actuators, B* **2018**, *269*, 15–21.
- (28) Luo, X.; Li, J.; Zhao, J.; Gu, L.; Qian, X.; Yang, Y. *Chin. Chem. Lett.* **2019**, *30*, 839–846.
- (29) Ren, H.; Huo, F.; Zhang, Y.; Zhao, S.; Yin, C. *Sens. Actuators, B* **2020**, *319*, 128248.
- (30) Luo, X.; Wang, R.; Lv, C.; Chen, G.; You, J.; Yu, F. *Anal. Chem.* **2020**, *92*, 1589–1597.
- (31) Long, S.; Qiao, Q.; Miao, L.; Xu, Z. *Chin. Chem. Lett.* **2019**, *30*, 573–576.
- (32) Wang, Y.; Yu, F.; Luo, X.; Li, M.; Zhao, L.; Yu, F. *Chem. Commun.* **2020**, *56*, 4412–4415.
- (33) Wang, Z.; Wu, H.; Liu, P.; Zeng, F.; Wu, S. *Biomaterials* **2017**, *139*, 139–150.
- (34) Sun, W.; Fan, J.; Hu, C.; Cao, J.; Zhang, H.; Xiong, X.; Wang, J.; Cui, S.; Sun, S.; Peng, X. *Chem. Commun.* **2013**, *49*, 3890–3892.
- (35) Zou, Y.; Li, M.; Xing, Y.; Duan, T.; Zhou, X.; Yu, F. *ACS Sens.* **2020**, *5*, 242–249.
- (36) Li, M.; Xing, Y.; Zou, Y.; Chen, G.; You, J.; Yu, F. *Sens. Actuators, B* **2020**, *309*, 127772.
- (37) Tang, Y.; Kong, X.; Xu, A.; Dong, B.; Lin, W. *Angew. Chem., Int. Ed.* **2016**, *55*, 3356–3359.
- (38) Wu, X.; Shi, W.; Li, X.; Ma, H. *Acc. Chem. Res.* **2019**, *52*, 1892–1904.
- (39) Mulay, S. V.; Kim, Y.; Lee, K. J.; Yudhistira, T.; Park, H.-S.; Churchill, D. G. *New J. Chem.* **2017**, *41*, 11934–11940.
- (40) Murale, D. P.; Kim, H.; Choi, W. S.; Churchill, D. G. *Org. Lett.* **2013**, *15*, 3946–3949.
- (41) Peng, T.; Chen, X.; Gao, L.; Zhang, T.; Wang, W.; Shen, J.; Yang, D. *Chem. Sci.* **2016**, *7*, 5407–5413.
- (42) Radi, R. *J. Biol. Chem.* **2013**, *288*, 26464–26472.

- (43) Lorsbach, R. B.; Murphy, W. J.; Lowenstein, C. J.; Snyder, S. H.; Russell, S. W. *J. Biol. Chem.* **1993**, *268*, 1908–1913.
- (44) Chang, C.; Zhao, Y.; Song, G.; She, K. *J. Neuroimmunol.* **2018**, *315*, 9–14.